

Decoding natural grasp types from human ECoG

Tobias Pistohl^{a,b,*}, Andreas Schulze-Bonhage^{a,c}, Ad Aertsen^{a,b}, Carsten Mehring^{a,b,1}, Tonio Ball^{a,c,1}

^a Bernstein Center Freiburg (BCF), 79104 Freiburg, Germany

^b Faculty of Biology, University of Freiburg, 79104 Freiburg, Germany

^c Epilepsy Center, University Medical Center Freiburg, 79104 Freiburg, Germany

ARTICLE INFO

Article history:

Received 7 February 2011

Revised 17 June 2011

Accepted 28 June 2011

Available online 8 July 2011

Keywords:

Grasping

Self-paced

Classification

ECoG

BCI

BMI

ABSTRACT

Electrocorticographic (ECoG) signals have been successfully used to provide information about arm movement direction, individual finger movements and even continuous arm movement trajectories. Thus, ECoG has been proposed as a potential control signal for implantable brain–machine interfaces (BMIs) in paralyzed patients. For the neuronal control of a prosthesis with versatile hand/arm functions, it is also necessary to successfully decode different types of grasping movements, such as precision grip and whole-hand grip. Although grasping is one of the most frequent and important hand movements performed in everyday life, until now, the decoding of ECoG activity related to different grasp types has not been systematically investigated. Here, we show that two different grasp types (precision vs. whole-hand grip) can be reliably distinguished in natural reach-to-grasp movements in single-trial ECoG recordings from the human motor cortex. Self-paced movement execution in a paradigm accounting for variability in grasped object position and weight was chosen to create a situation similar to everyday settings. We identified three informative signal components (low-pass-filtered component, low-frequency and high-frequency amplitude modulations), which allowed for accurate decoding of precision and whole-hand grips. Importantly, grasp type decoding generalized over different object positions and weights. Within the frontal lobe, informative signals predominated in the precentral motor cortex and could also be found in the right hemisphere's homologue of Broca's area. We conclude that ECoG signals are promising candidates for BMIs that include the restoration of grasping movements.

© 2011 Elsevier Inc. All rights reserved.

Introduction

Brain–machine interfaces (BMIs) are being widely discussed as a possible means for helping severely paralyzed patients to regain neuronal control over prosthetic limbs (Velliste et al., 2008) or even their own paralyzed limbs via functional electric muscle stimulation (Moritz et al., 2008).

Since it has been shown that not only spike (action potential) recordings but also continuous signals such as the local field potential (LFP) and the electrocorticogram (ECoG) can be used to infer movement intentions from the motor cortex (Ball et al., 2009a; Leuthardt et al., 2004; Mehring et al., 2003; Pistohl et al., 2008; Schalk et al., 2007; Stark and Abeles, 2007), the ECoG has been proposed as a potential control signal for BMIs (e.g., Ball et al., 2004; Levine et al., 2000; Leuthardt et al., 2006; Mehring et al., 2004; Schalk et al., 2008a). An ECoG-based BMI might exhibit several advantages: compared to spike recordings, measurements do not require implantation of

intracortical electrodes, compared to non-invasive techniques, such as extracranially recorded electroencephalography (EEG) or magnetoencephalography (MEG), it exhibits higher spatio-temporal resolution, superior signal-to-noise ratio, in particular in high frequencies, and is less prone to artifacts (Ball et al., 2009b). ECoG recordings are used in patients for pre-surgical epilepsy diagnostics, which makes it possible to conduct ECoG studies with human subjects.

One concept for BMI applications, which has first been pursued for intra-cortical spike recordings, is to use cortical activation patterns as generated during voluntary control of healthy limbs to control equivalent movements of an artificial effector. If ECoG recordings are to be used in this manner, their potential for correct and reliable decoding of real movements has to be proven. This has been already achieved for classification of movement directions (Ball et al., 2009a; Leuthardt et al., 2004; Mehring et al., 2004), finger movements (Ball et al., 2004; Miller et al., 2009), and for predicting continuous trajectories of hand–arm movements (Chao et al., 2010; Gunduz et al., 2009; Pistohl et al., 2008; Schalk et al., 2007). Perfect accuracy in offline decoding may not be necessary in order to exploit the decoding of natural movement patterns in long-term online BMI applications, as performance can still be improved by neural adaptation to the properties of a BMI (e.g., Taylor et al., 2002).

* Corresponding author at: Faculty of Biology, University of Freiburg, 79104 Freiburg, Germany.

E-mail address: tobias.pistohl@bcf.uni-freiburg.de (T. Pistohl).

¹ These authors contributed in equal parts.

For the control of a hand-arm prosthesis, it is essential to decode hand movements. Studies in monkeys have demonstrated successful one-dimensional control of a gripping device using spike signals from the motor cortex (Carmena et al., 2003; Velliste et al., 2008). As of yet, however, opening and closing movements have been implemented without distinguishing between different grasp types.

Previously, it has been shown that it is possible to decode individuated finger movements from human ECoG (Kubánek et al., 2009; Miller et al., 2009). Whether a strategy aimed at decoding multiple finger movements performed simultaneously can be successful, and if it would allow reproducing well-coordinated grasping movements in natural movement settings, is, however, currently unclear. Such decoding might be difficult to achieve as different ways of grasping an object can involve the same types of finger movements, such as flexing all the fingers at the same time, both in whole-hand and precision grips, but with different patterns of inter-finger coordination. Therefore, we took a different approach: an appropriate control scheme for hand prostheses with many degrees of freedom or artificial re-innervation of hand muscles by functional electrical stimulation does not necessarily need to control every single joint separately. Natural grasping involves a large number of synergies (Mason et al., 2001; Santello and Soechting, 2000; Thakur et al., 2008), which may also be represented in the neural control of natural hand movements (Schieber and Hibbard, 1993; Zatsiorsky et al., 2000). A BMI for grasping might therefore rather use high-level commands that activate several actuators or muscle groups in coordination. Among the most basic and most important of such high-level commands would be the ones initiating grasps for interaction with different objects.

Therefore, we aimed to investigate the use of ECoG signals for motor decoding of different hand configurations in a scenario close to an everyday environment, as this might be the venue of possible BMI applications. The experimental design we created for this purpose allowed for grasps within a sequence of natural, continuous self-paced movements. To cover some of the variability innate to the natural use of the human hand and arm, it used a wide workspace with objects to be grasped at different angular positions and requiring different hand forces. In the course of the movement sequence, two different grasp types were applied by the subjects on a familiar object (a mid-sized cup): precision grip and whole-hand grip. We investigated whether the ECoG signals recorded during this grasping task constituted a reliable neural signal for controlling a grasping prosthesis. In particular, we investigated which signal components were informative about grasping movements, and, based on precise assignment of electrode positions to the cortical brain anatomy of the patients, from which cortical areas they could be recorded.

Methods

Motor task

The motor task chosen for this study was designed to allow for natural movement sequences of reaching and grasping. A table-like platform was placed in front of the subjects sitting upright in a hospital bed. A plastic cup could be placed in one of four different positions, marked by circles, arranged in a semi-circle around a central point. The distance between neighboring positions was 15.6 cm. A different sign (a pictograph of a hand) marked the central resting position. The task sequence is outlined in Fig. 1.

Three-dimensional hand positions were continuously tracked by a system (Zebris, Isny, Germany) using markers on the patients' wrists (over the radial styloid process) emitting ultrasound pulses recorded by a set of sensors.

A movement trial started when the subjects (referred to as S1, S2 and S3) reached out, at a time of their own choosing, from the resting position to a plastic cup situated at one of the four peripheral positions, grasped it and relocated it to a new position, self-chosen

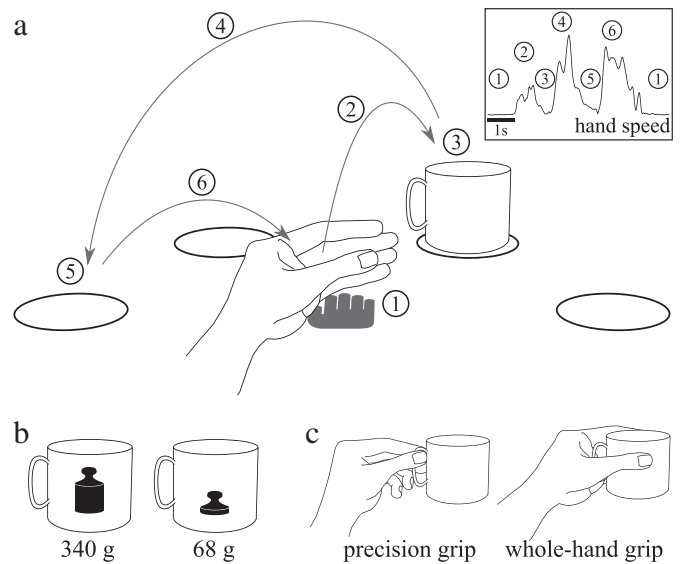


Fig. 1. Reach-to-grasp experiment. (a) Layout and time course of the self-paced movement sequence. From a central resting position (1), marked by a hand pictograph (here seen in perspective view), the subjects reached for a cup (2) located at one of four predefined positions marked by circles. Without interrupting the movement, the cup was grasped, picked up from the table (3) and carried (4) to another of the four positions (self-chosen by the subject) and released there (5). After that, the subjects returned their hand (6) to the starting position and waited several seconds before initiating, at a time of their own choice, the next movement sequence. Hand position was recorded via an ultrasound emitter attached to the wrist. The small inset in the upper right corner shows an example of a hand speed profile during one trial, with stages of the movement sequence marked (1–6). (b) Each 15–16 trials, the cup was exchanged, alternating between a light and a heavy version. (c) In each trial, the subject arbitrarily decided whether to use a precision grip on the handle of the cup or a whole-hand grip on the whole cup.

from the three remaining positions. After the cup was put back on the table, the hand was returned to the central resting position. This ended the trial, and the subjects waited for some time before initiating the next trial. Information on actual timing within and across trials is summarized in Table 2.

In each single trial, the subjects decided whether to apply a precision grip or a whole-hand grip. The precision grip was performed by grasping the cup by the handle between the thumb and the index finger, supported by the other fingers, while the whole-hand grip was performed by closing the hand around the whole cup (cf. Fig. 1c). When one grasp modality seemed under-represented during a running experimental session, the subjects were instructed to use this grasp type more often. However, such instructions needed only to be given once or twice per subject.

To control for the application of different hand forces, for every new block of 15 (S1) or 16 (S2 and S3) trials, the cup was switched between two, otherwise identical, versions of different weight. The lighter cup weighed 68 g (2.4 oz), while the heavier one, with a metal weight fixed to the inside of the cup, was 5 times as heavy, weighing 340 g (12 oz).

Although, across trials, there was considerable variability in the applied hand configurations, even within the same subject and grasp type (e.g., due to corrective movements made to align the hand properly to the handle of the cup), no trials were excluded from the analysis for such reasons, as the present study aimed to investigate the possibility of decoding grasp type in the presence of a natural degree of variability, as can be expected in daily life situations.

Subjects

The experiment was conducted with three human subjects (all female, aged 14–16) suffering from intractable epilepsy and

undergoing pre-neurosurgical diagnosis by means of ECoG. All subjects were right-handed, but they were asked to use the hand contralateral to the electrode implantation site (cf. Table 1). The study was approved by the Ethics Committee of the University Medical Center Freiburg and conducted after the subjects and their parents (since subjects were underage) gave their written informed consent.

Neural recordings

All subjects had implanted stainless-steel electrodes (Ad-Tech, Racine, Wisconsin, USA) of a 4 mm diameter, covered in sheets of silicone and arranged in regular grids (cf. Table 1) with a 10 mm center-to-center distance. S2 had additional inter-hemispheric stripes, which were not used for data analysis. Electrode arrays were subdurally implanted over the lateral convexity of the subjects' cortices, partially covering the precentral motor cortex.

For S1 and S2, ECoG was recorded using a clinical EEG-System (IT-Med, Germany) and sampled at a rate of 256 Hz (S1, S2) using a high-pass filter with a 0.032 Hz cutoff frequency and a low-pass filter at 95 Hz. The same monitoring system with different amplifiers was used for S3, sampling at 1024 Hz while applying high- and low-pass filters at 0.032 Hz and 379 Hz, respectively. For all subjects, digital video recordings (25 Hz frame rate), synchronized to the ECoG signals, were acquired.

Electrical stimulation through the electrode grid was performed using an INOMED NS 60 stimulator (INOMED, Germany). Trains of a 7 s duration consisted of 50 Hz pulses of alternating-polarity square waves of 200 μ s each. The intensity of stimulation was gradually increased up to 15 mA or to the induction of sensory and/or motor phenomena. The patients were unaware of the timing of stimulation, unless any motor-, sensory- or speech-related symptoms occurred. All sites with arm or hand motor responses were, in all subjects, located outside the ictal onset zone.

In each subject, a structural MRI data set with full head coverage and 1 mm \times 1 mm \times 1 mm resolution was acquired, both before and after electrode implantation, using a T1 MPRAGE sequence. The motor cortices were identified according to anatomical landmarks (Rumeau et al., 1994; Steinmetz et al., 1989; Yousry et al., 1997). Individual locations of the central and lateral sulci, as determined from the post-implantation MRI, were used to assign the electrodes to the frontal, parietal and temporal lobes using a probabilistic atlas system (Eickhoff et al., 2006) based on the maximum-probability assignment of the cortical position immediately beneath an electrode contact (i.e.,

perpendicular to the electrode surface). The probabilistic maps used were part of the SPM Anatomy Toolbox Version 1.7b. Electrode positions were visualized in the pre-implant MRI as described by Kovalev et al. (2005).

In addition to the intracranial ECoG, classical scalp EEG was recorded using either 19 (S1) or 21 (S2 and S3) scalp electrodes, as well as horizontal and vertical EOG (electrooculogram).

The choice of electrode implantation sites, electrical stimulation, MRI acquisition and other measures described in this section were dictated solely by clinical requirements.

Data analysis

Assignment of events

Since the performance of the motor task was completely self-paced, individual events constituting a grasping movement, i.e., movement onset, grasp onset, release of the cup, and movement end had to be identified post-hoc on a single-trial basis. For S1 and S3, hand position recordings obtained synchronously to the neural data were used for this purpose. Both grasp onset and cup release were marked by local minima in the speed profile of the hand (see inset in Fig. 1a) by a local minimum in height and a turn in position parallel to the surface of the table, as these events corresponded well to the times of grasp onset and cup release. For S2, wrist position recordings could not be accurately synchronized to the neural recordings, and the synchronously acquired video recordings were used to identify the above-mentioned events. Here, 'grasp onset' refers to the time when the grip was tightened, shortly before the subjects lifted the cup, and not when they first touched it or when the hand was pre-shaped for the grasp during the reaching movement, which, in fact, could occur as early as at movement onset.

In total, 961 trials were recorded from S1, S2 and S3. The average duration of a trial, from movement start to movement end, was 3.7 ± 0.6 s (mean \pm standard deviation) with a 1.2 ± 0.7 s pause between successive trials of one block of 15 (S1) or 16 (S2, S3) successive grasps. The average time from movement onset to grasp onset was 1.1 ± 0.3 s (Table 2).

Signal-to-noise ratio

The signal-to-noise ratio (SNR) allows to assess the strength of a specific signal relative to corrupting noise (e.g., caused by variability in task execution). For the comparison of time- and frequency-resolved ECoG amplitudes from the two grasp types, we used the SNR, defined by the difference of the class means (as an estimate of the signal) divided by the average trial-by-trial fluctuations within classes (as an estimate of noise):

$$\text{SNR} = \frac{|\mu_1 - \mu_2|}{0.5 \times (\sigma_1 + \sigma_2)}$$

where μ_1 and μ_2 are the means of the two classes of grasping movements; σ_1 and σ_2 are their standard deviations across trials.

Table 1

Subject overview. All subjects were female and had ECoG electrodes subdurally implanted for pre-neurosurgical diagnosis. FCD = focal cortical dysplasia.

	S1	S2	S3
Age (years)	14	16	15
Handedness	Right	Right	Right
Pathology	Right frontal FCD	FCD in right superior frontal gyrus/right cingulate gyrus	Right frontal FCD
Implanted electrodes	Fronto-parietal 8 \times 8 grid; 3 lateral prefrontal stripes (1 \times 6 contacts); 1 anterior cingulate depth electrode (10 contacts); 1 medial fronto-polar depth electrode (10 contacts); all electrodes on the right	Fronto-parietal 6 \times 8 grid; 3 inter-hemispheric stripes (1 \times 4 contacts); all electrodes on the left	Right fronto-parietal 8 \times 8 grid
Seizure onset zone	Right medial and lateral prefrontal	Left inter-hemispheric	Right premotor

Table 2

Behavioral data for each subject (S1, S2, S3). Number of trials, average duration of trials, time from movement start to grasp onset, and inter-trial intervals (ITI) (excluding breaks between blocks of 15 or 16 trials, which were longer). Times are given as averages in seconds and standard deviation in parentheses. The last column ('all') gives the same numbers over all trials of all subjects.

	S1	S2	S3	All
Number of trials	303	338	320	961
Duration (s), mean (σ)	4.2 (0.6)	3.3 (0.5)	3.5 (0.5)	3.7 (0.6)
Start to grasp (s), mean (σ)	1.1 (0.3)	1.0 (0.3)	1.2 (0.4)	1.1 (0.3)
ITI (s), mean (σ)	1.0 (0.3)	2.0 (0.5)	1.0 (0.3)	1.2 (0.7)

Preprocessing of neural data

General treatment of recordings. Prior to more specific processing, all neuronal activity data was re-referenced to a common average reference of all grid channels indicated in Fig. 2. Additionally, for each recorded channel, the average voltage over the whole data block (usually one hour) was subtracted to eliminate any possible offset of the data. Then, to normalize for systematic differences in amplitudes across channels, the signal from each channel was divided by its standard deviation over the entire block of data. Otherwise, covariance matrices estimated from very differently scaled channels could become ill-conditioned, leading to inaccurate results during matrix inversion (cf. Decoding).

Spectral amplitudes. All frequency-resolved data used in this study were generated via a multi-tapering method (Thomson, 1982) applied to successive overlapping 250 ms windows of the recorded ECoG signals, moved in steps of 125 ms. This resulted in a frequency binning of 4 Hz and a temporal sampling rate of 8 Hz for the estimates of spectral amplitudes. Multi-tapering methods yield a statistically consistent spectral estimator, with improved localization in the frequency domain and reduced variance of the spectral estimates. To this end, the ECoG signal from each time window was first multiplied by a window function (a taper) and then Fourier-transformed. Multiple taper functions, orthogonal to each other, were used and a weighted average was applied to the resulting spectrograms. We used Slepian taper functions (Percival and Walden, 1993), which yield optimal localization in the frequency domain. The effective frequency resolution is reduced by this method, depending on the number of tapers used. We used three Slepian tapers, corresponding to a frequency resolution with a half-bandwidth of 8 Hz.

To account for the large variations in spectral power over different frequencies, in particular decreasing power with increasing frequencies, each frequency bin was normalized to, i.e., divided by, the trial- and time-averaged amplitude value of this frequency bin during a baseline period. The baseline period consisted of intervals of 0.75 s (6 time windows), from 1 s to 0.25 s before movement onset. This normalization procedure is not only valuable for the presentation of spectral modulations over a large frequency range, but is especially important when averaging amplitudes over broad frequency bands. Without such normalization, high frequencies with low power but not necessarily low signal-to-noise ratio (cf. Results, Movement-related

potentials and spectral amplitude modulations), would be under-represented in the average across a broad frequency band.

Since information from normalized amplitude modulations over adjacent frequency bins within broader frequency bands can be assumed to be highly correlated, we averaged normalized amplitudes over a number of adjacent frequency bins, both to reduce the dimensionality of the feature space and to increase the signal-to-noise ratio. We concentrated most of our analyses on amplitude modulations in three distinct frequency bands that were modulated during the motor task (cf. Results, Movement-related potentials and spectral amplitude modulations) and also yielded good decoding results (cf. Results, Classification of grasp types).

Low-pass filtered component (LFC). ECoG was consistently modulated in a low-frequency band (<6 Hz, cf. Results, Classification of grasp types) during task execution. To extract this signal component, we applied a low-pass filter to the raw signals with a cut-off frequency of approximately 5 Hz. In contrast to analyses based on amplitude modulations (see above), this procedure retains phase information of the signals. Moreover, the low-pass filtered component (LFC) had been already successfully used for motor decoding in earlier EEG, MEG, LFP and ECoG studies (Ball et al., 2009a; Mehring et al., 2003; Pistohl et al., 2008; Rickert et al., 2005; Schalk et al., 2007; Waldert et al., 2008; see also Waldert et al., 2009 for a review). Furthermore, Jerbi et al. (2007) have shown that MEG in a 2–5 Hz range was phase-locked to the time-varying speed of the hand, indicating a direct relationship between hand movement and a low-frequency component of cortical potentials.

To extract the LFC, we applied a 2nd order Savitzky–Golay filter (Savitzky and Golay, 1964) of 250 ms width, mainly retaining frequencies below 5 Hz (frequency response dropped below –3 dB), to the ECoG recordings. While Savitzky–Golay filters do not have a well-defined cut-off frequency, they preserve local minima and maxima of the original signal better than other low-pass filtering methods and may be seen as a good smoothing tool.

Decoding

Algorithm. We used a regularized version (Friedman, 1989) of linear discriminant analysis (Hastie et al., 1995) to classify the trials from the recorded ECoG activity. For each class of movements (e.g., grasp modality: precision grip or whole-hand grip), an N -dimensional Gaussian distribution was fitted to the N -dimensional feature vector

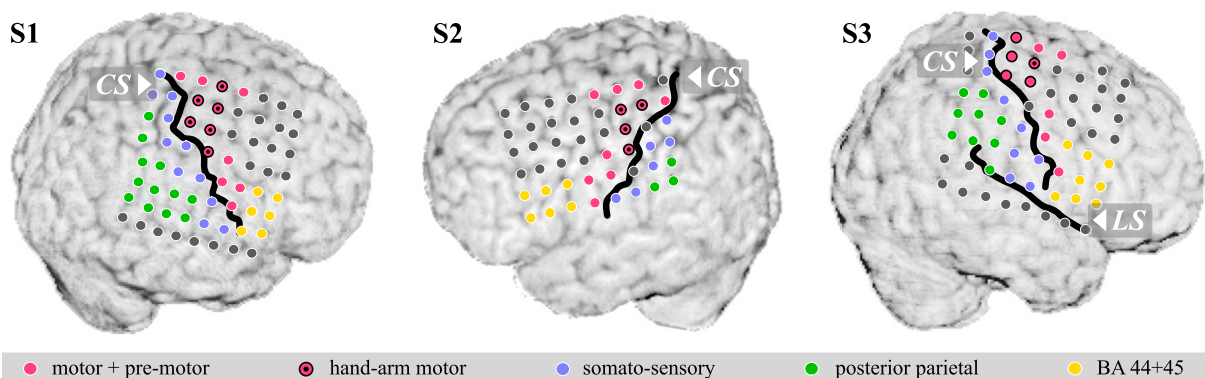


Fig. 2. Location and functional electrical stimulation results of subdurally implanted ECoG electrodes. From left to right: subjects S1, S2 and S3. Gray or colored dots indicate locations on the ECoG grid that were identified as being over motor/pre-motor areas (magenta), somato-sensory (blue), posterior parietal (green), Brodmann areas 44 and 45 (yellow). Frontal electrode sites where electrical stimulation evoked hand or arm movements are marked by black outlines and a black dot in the center of the electrode symbol (these hand-arm motor channels were used for decoding in the main analyses). Locations of the central sulcus (CS) and the lateral sulcus (LS, S3 only) relative to electrode positions were determined from the individual post-implant MRIs (marked by solid black lines).

samples of all trials within a predefined training set. We used common covariance matrices for all classes but class-dependent means (assumption of linear discriminant analysis). To avoid overfitting, regularization was applied, imposing restrictions on the covariance matrix by interpolating between the maximum likelihood estimate of the covariance matrix Σ and the scalar covariance (Friedman, 1989):

$$\hat{\Sigma}(\gamma) = (1-\gamma)\Sigma + \frac{\gamma}{N}\text{tr}(\Sigma)I$$

where I denotes the identity matrix and $\text{tr}(\Sigma)$ – the trace of Σ . The degree of interpolation is specified by the regularization parameter γ to obtain the regularized covariance $\hat{\Sigma}(\gamma)$.

For each feature vector representing a trial from the test set, we computed the posterior probability for each class by Bayes' theorem using a homogeneous prior and chose the class with the highest posterior probability. The percentage of correctly decoded trials is referred to as the decoding accuracy (DA). To account for the possibility of different sample sizes of each class in the test set, we calculated the DA for each class separately and then averaged it over classes. Whenever DA is presented, we refer to this normalized version.

Feature vectors. For use in an automated classifier, neuronal signals are usually reduced to a set of features that capture the characteristics of the different classes. One crucial factor in the decoding process is the choice of signal features used for classification. Generally, feature optimization, as through improved channel selection (Lal et al., 2004) or spatial filtering methods like common spatial patterns (CSP; Müller et al., 2000; Ramoser et al., 2000) could greatly improve decoding in EEG-based studies and might also be considered for ECoG data. Our investigation, however, was not focused on subject-specific optimization, but instead employed a selection of features, common for all subjects.

Characteristics of the neural movement-related activity were gathered in a vector of signal features using (i) values of one or several signal components, (ii) measured at one or more ECoG electrodes, (iii) at one or several time points in relation to the grasping event. The choice of ECoG channels (ii) and time points (iii) was based on the anatomical and functional assignment of the electrodes and the typical timing of the reach-to-grasp movements (cf. Table 2). No further optimization for informative signals was performed in order to provide a consistent and transferable scheme of feature selection that could be applied without calibration.

This procedure yielded one feature vector per trial comprising a maximum of 168 values, depending on the subject and the intended analysis (maximum reached for S1: 6 channels, 4 signal components, 7 time points; $6 \times 4 \times 7 = 168$ feature dimensions, less for S2 and S3 because of lower number of channels; see Section 3.2).

Evaluation of decoding performance. Ten-fold cross-validation was used to evaluate decoding performance: the trials were randomly assigned to ten different sets of equal size, nine of which were grouped to fit the model parameters (training set). The remaining one tenth of the trials were used to apply the classifier and evaluate the performance of the decoding against real labels (test set). Subsequently, the test set was switched to another subset of trials, so that, after ten repetitions, each trial took part in a test set exactly once. To improve estimation, this procedure was repeated several times with different random assignments of the trials to the subsets. If not stated otherwise, DAs are given as the average over 20 repetitions of a ten-fold cross-validation.

To choose an appropriate value for the regularization parameter γ , within each cross-validation step, a number of secondary ten-fold cross-validations were run on the current training set, testing

different values of γ (10^{-4} and 0.1 to 1 in steps of 0.1). The value yielding the best decoding was used to retrain the model on the basis of the complete training set. Thereby, in each cross-validation step, the regularization parameter was optimized on the basis of the training data only.

To test for significance, we assumed a null hypothesis of random assignment with equal probabilities for each of the two classes (chance level: 50%). Resulting chance predictions can be described by a binomial distribution. From the cumulative binomial distribution, an upper limit of DAs (upper significance level), to cover a portion of $1-\alpha$ of chance decodings, can be inferred ($p < \alpha$). Since in a set of multiple tests, it becomes more likely to observe DAs above the identified significance level by pure chance, the α level was adjusted using a Bonferroni correction when necessary (see Results).

Results

Most of our analyses focused on measurements from electrodes implanted over the hand-arm motor cortex. The hand-arm motor cortex was defined as the precentral region where electrical stimulation mapping showed hand and/or arm motor responses. Channels located posterior to the central sulcus, as determined from the subjects' individual MRI data sets, were excluded from the analysis to reduce the impact of responses from the postcentral somato-sensory cortex.

Movement-related potentials and spectral amplitude modulations

Fig. 3a shows, for all three subjects, the time-resolved amplitude spectra from one representative channel from the hand-arm motor cortex. Recordings were averaged over all trials of one type of grasp (top row: precision grip, second row: whole-hand grip) for frequencies from 0–128 Hz relative to a baseline period before each trial (cf. Methods, Preprocessing of neural data). Clear modulations, both reduction and increase in amplitudes, can be observed in very low frequencies below 6 Hz. A longer-lasting reduction of amplitudes, starting well before and ending well after a grasp, can be observed in the alpha and beta ranges, as is typical for any motor task. A similar but smaller power drop was found in higher frequencies up to almost 50 Hz. Finally, in a broad band of high frequencies from 54 Hz up to over 100 Hz, a consistent amplitude increase can be observed around the grasp, with a second, smaller peak at the time of cup release (as could be confirmed by aligning recordings to this time, see supplementary material, Fig. SUP6). For S3, whose signals were recorded at a higher sampling rate and with different filter settings (cf. Methods, Neural recordings), this increase continued to even higher frequencies. S1 and S2 showed the strongest responses below 100 Hz – in these two subjects, however, frequencies above 128 Hz could not be examined, since signals were sampled at a rate of only 256 Hz (S3: 1024 Hz).

Next, we asked how differentiable ECoG activity for different grasp types (precision grip and whole-hand grip) was. For this purpose, we determined the signal-to-noise ratio (SNR) of the ECoG spectrograms as the ratio of the differences of the means for both grasp types to the mean variability (standard deviation) across trials (cf. Methods, Data analysis). For the ECoG spectrograms of one channel per subject recorded from the hand-arm motor cortex the SNR for the two grasp types, resolved over time and frequency, is shown in Fig. 3b. A consistent property over subjects was the almost negligible SNR in the intermediate-frequency bands that showed an amplitude reduction during task execution, whereas modulations in the low- (≤ 6 Hz) and high-frequency (≥ 54 Hz) bands had much higher SNR. Note that the SNR for S2 was considerably lower than for S1 and S3; higher SNR values for S2 were only found on channels, recorded over the somato-sensory cortex.

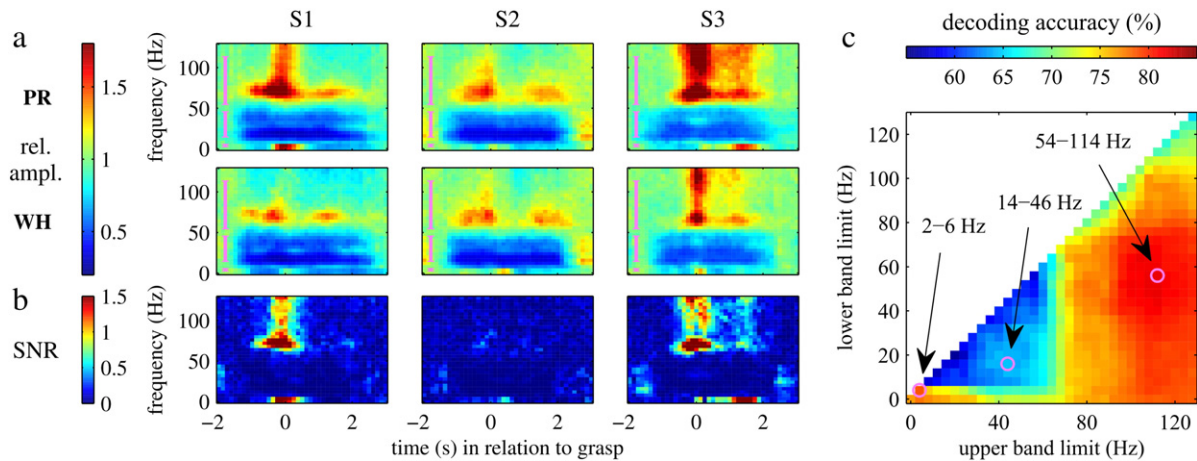


Fig. 3. Spectro-temporal modulations of the ECoG signals during the task. (a) Average spectrograms of normalized ECoG amplitudes, aligned to grasp onset (cf. *Methods, Data analysis*) from a representative channel over the hand-arm motor cortex of each subject (S1–S3, from left to right). Top row: precision grip (PR), second row: whole-hand grip (WH). Pink bars in the left of the frames mark the frequency bands used for decoding. (b) Signal-to-noise ratio (SNR, cf., *Methods, Data analysis*), resolved in time and frequency, obtained from the spectrograms of the same channel as in (a). (c) Scan over continuous frequency bands of different width and location for decoding of grasp type (precision grip vs. whole-hand grip), averaged over subjects. Decoding was evaluated on the amplitudes averaged across all frequency bins between a lower (vertical axis) and an upper (horizontal axis) limit. The resulting average DA is color-coded for each possible contiguous frequency band. Decoding was based on neuronal features gathered from the frequency-band modulations of all hand-arm motor cortex channels at seven different time points, evenly distributed over an interval of 1 s before to 0.5 s after grasp onset. Pink circles mark frequency bands used for decoding (cf. pink bars in (a)) in the remainder of this study.

These results (Figs. 3a–b) suggest a range of possible signal components to be used for decoding. On a coarse scale, three frequency bands seem to play distinctive roles during grasping: a low-frequency band showing either amplitude increase or decrease a high-frequency band showing amplitude increase, and an intermediate-frequency band, displaying a more sustained amplitude decrease, which, in turn, could be divided into lower and higher, possibly functionally different, sub-bands. However, from this, it is not obvious whether a further subdivision into narrower – or different – frequency bands could be beneficial for decoding grasp types. Therefore, all possible continuous frequency bands, i.e., averages over sets of neighboring frequency bins (cf. *Methods*), were tested for their potential applicability (Fig. 3c, discussed in *Classification of grasp types*), by decoding on the basis of each of these bands, respectively.

We selected three frequency bands, based on the local maxima in Fig. 3c, for more detailed analyses. The definition of these bands was consistent with observations made on the basis of task-related relative amplitude modulations (Fig. 3a):

- (1) a low-frequency band: 2–6 Hz,
- (2) an intermediate-frequency band: 14–46 Hz, and
- (3) a high-frequency band: 54–114 Hz.

To examine amplitude modulations within each of these frequency bands, normalized amplitude values were averaged over all enclosed frequency bins.

Figs. 4a–c show, for a set of neighboring electrodes and for each grasp type, the averaged normalized amplitudes in each of the three frequency bands defined above, during task execution. Very clear differences between the two grasp types can be observed in the low- (Fig. 4a) and high-frequency bands (Fig. 4c). This holds for several channels recorded over hand-arm areas of the motor cortex, with different channels exhibiting grasp specificity in different features of the signals (amplitude, timing, or both), which could potentially provide non-redundant information. Differences in the intermediate-frequency band (Fig. 4b) were much smaller, as could be expected from the time-frequency-resolved SNR (Fig. 3b).

Fig. 4d shows trial-averaged potentials of the low-pass-filtered ECoG component (LFC; cf. *Methods*) for both grasp types. Other than the amplitude modulations of the frequency bands described above, the LFC also includes phase information and allows for larger grasp-

specific differences, since movement-related potentials may have opposite signs for different grasp types.

Classification of grasp types

When using amplitude modulations in different frequency bands of the ECoG to decode grasp movement classes, there is no obvious rule, which frequency bands should be used and how many different frequency bands should be differentiated (cf. *Movement-related potentials and spectral amplitude modulations*). Therefore, we tested the performance of decoding on the basis of a wide variety of frequency bands in the range of 0 to 128 Hz. For this purpose, we constructed a feature vector for each trial from amplitude values of the examined band taken from a time interval ranging from -1 s to $+0.5$ s in relation to grasp onset in each trial. This temporal range roughly corresponded to the first epoch of high-frequency activation related to the grasp (Fig. 3a). Within this interval, values were picked every 250 ms to obtain samples from non-overlapping and thus more independent analysis windows of the spectrogram (cf. *Methods, Preprocessing of neural data*). For each band, a ten-fold cross-validation with mutually exclusive test and training sets was repeated 20 times (cf. *Methods, Decoding*).

Fig. 3c presents the average decoding accuracy (DA) over all repetitions and all subjects for all investigated frequency ranges sorted for their respective lower and upper frequency limits. Generally, broader frequency bands (points farther from the diagonal in Fig. 3c) yielded a higher DA than narrow frequency bands (points closer to the diagonal). The low- and high-frequency bands, as described in section "*Movement-related potentials and spectral amplitude modulations*", corresponded to local maxima in Fig. 3c. A much lower DA was achieved using bands from the intermediate-frequency range. However, a local maximum of relatively low amplitude was also found in a band encompassing the beta and low gamma range (14–46 Hz). Bands comprising the alpha- and beta-range frequencies (6–26 Hz) were least informative with regard to decoding grasp types from ECoG signals.

Based on the results in Figs. 3a–c, we restricted all further analyses to the frequency bands discussed in Section 3.1 (low, intermediate and high) as well as to the LFC.

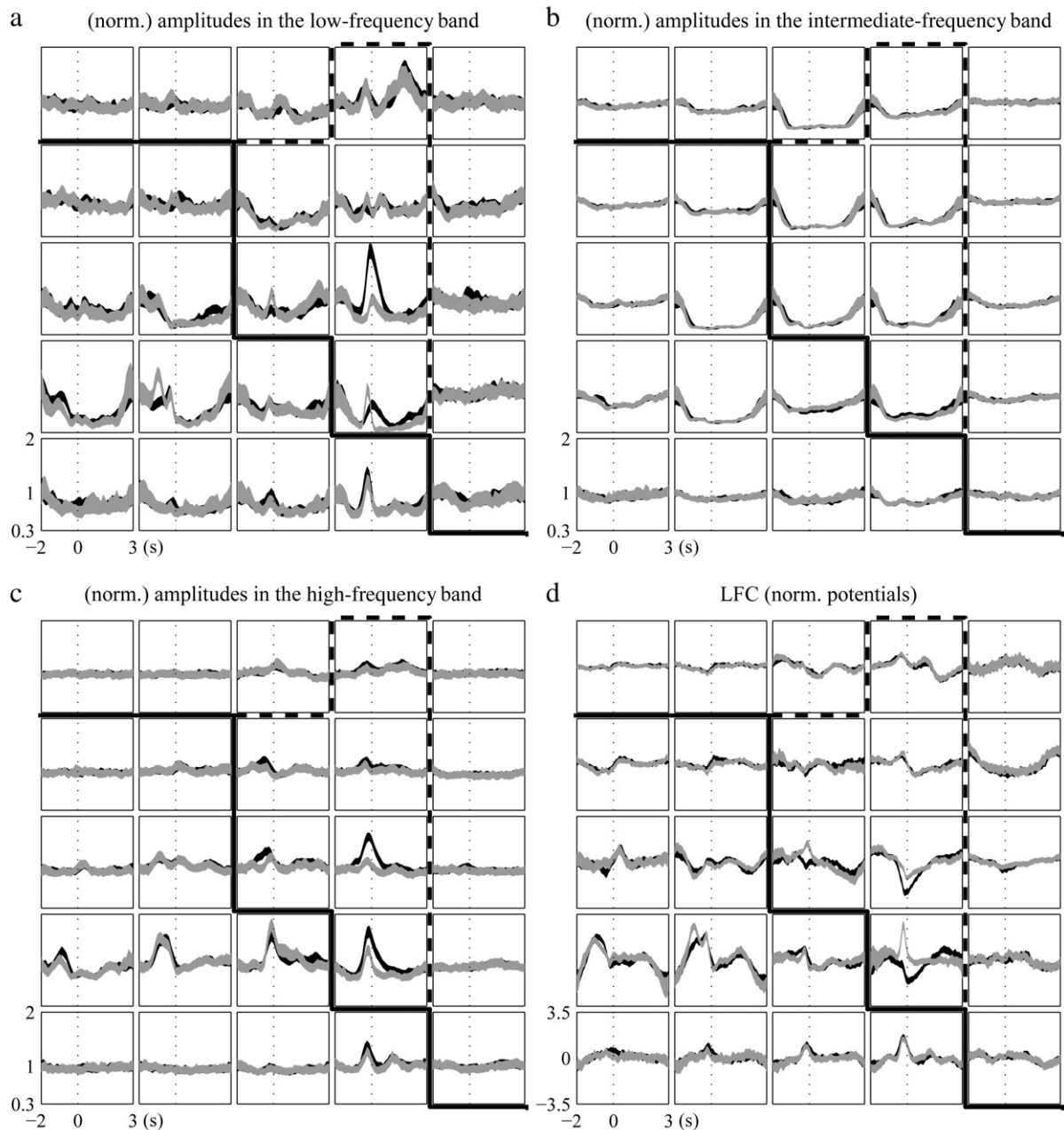


Fig. 4. Average modulations ($\pm 3 \times$ standard error of the mean) of different neuronal signal components over the course of a movement sequence aligned to grasp onset for precision grip (black) and whole-hand grip (gray). Signals are exemplarily shown for a subset of electrodes from S1 (equivalent illustrations for S2 and S3 in Figs. SUP4 and SUP5). (a) Normalized amplitude modulations in the frequency bands of 2–6 Hz, (b) 14–46 Hz, (c) 54–114 Hz, and (d) potentials of the low-pass-filtered component (LFC). Channels are presented in a topographical manner as they were located in the electrode grid. Solid lines separate electrode positions posterior (lower left) and anterior (upper right) to the central sulcus; electrodes on the hand-arm motor area are marked by a dashed outline.

A summary of the average DA of all three subjects is shown as groups of three bars for each kind of feature combination in Fig. 5a. Variability over 20 repetitions of the cross-validation is indicated by small black bars in the graph, depicting standard deviation. Please note that this should not be translated into confidence intervals of DA, since results for repetitions are not statistically independent.

We used the spatio-temporal pattern of the features described above (hand-arm motor channels, 1 s before to 0.5 s after grasp time) for each of the four signal components (low, intermediate, high, LFC), and their combinations. Three particularly notable combinations were included into Figs. 5a,b. On average, the LFC yielded a higher DA than any of the three amplitude signals or any combination of amplitude signals. The most successful of the amplitude signals was the high-frequency band, closely followed by amplitudes in low frequencies.

Amplitudes in the intermediate-frequency range yielded a significant but very low DA. A slight increase in performance from the LFC alone could be achieved by adding low- and high-frequency amplitudes to the feature vector. Further enlargement of the feature vector by adding amplitude values from all three frequency bands did not increase performance. While predictions for S1 and S3 were very accurate, reaching 97.1% and 97.2% DA, respectively, the performance for S2 yielded a lower DA of 84.0%. Note that channels recorded posterior to the central sulcus were excluded from the analyses to reduce sensory input.

The time-resolved DA of the signals in relation to the grasping event was evaluated by using signal vectors composed of all hand-arm motor channels assembled from one specific time point in a trial, repeated for all time points during the entire duration of a typical trial

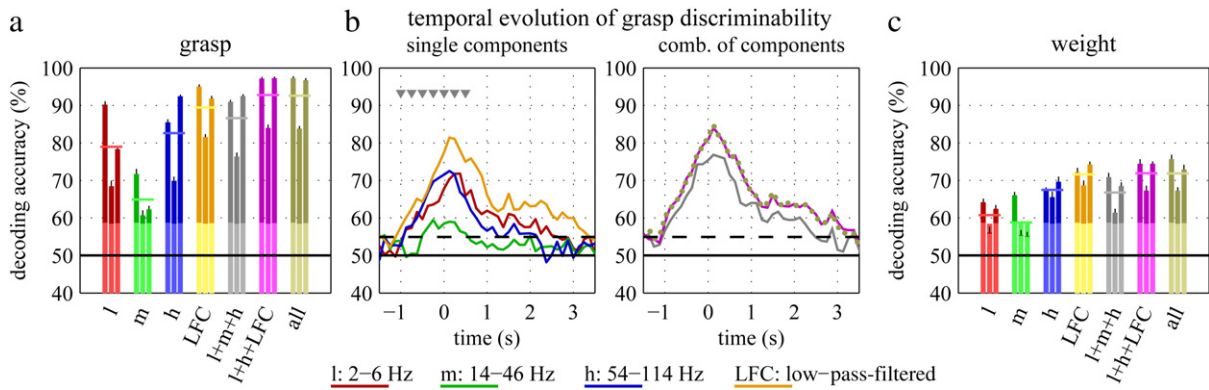


Fig. 5. Decoding accuracy (DA). (a) Classification of the two grasp types using different signal components: l: amplitudes of a low-frequency band (2–6 Hz), m: amplitudes of an intermediate-frequency band (14–46 Hz), h: amplitudes of a high-frequency band (54–114 Hz), LFC: low-pass-filtered potentials. Additional bars represent combinations of these signal components. In all cases, a temporal pattern of samples (seven samples at different time points indicated by gray triangles in (b)) from each hand-arm motor channel was used. Each triplet of bars of one specific color represents the decoding results from a specific signal component or a combination thereof for subjects S1, S2 and S3 (left to right). The average over subjects is marked by the correspondingly colored horizontal lines. The black horizontal line indicates chance level (0.5) below significance level ($p < 0.001$) bars are displayed in pale colors. Small black bars on top indicate standard deviation over 20 repetitions of the cross-validation. (b) Temporal development of the DA (across trials of all subjects), using samples from hand-arm motor channels at only one time point (horizontal axis) with relative to grasp onset. Results for single signal components (l, m, h and LFC) are depicted in the left panel of (b). The significance level is given by a dashed line. The right panel of (b) shows the same for combinations of different signal components. Colors for signal types and combinations thereof are the same as in (a). (c) Decoding of different object weights – same form of presentation as in (a), but calculated with different frequency band limits (see text: low: 0–10 Hz, intermediate: 14–26 Hz, high: 74–118 Hz), and the temporal pattern shifted to later in the trial (between 0.5 s before and 1 s after grasp onset).

(from about 1 s before to 3 s after grasp onset). DAs, calculated over all decoded trials from all subjects, as shown in Fig. 5b, indicate that the peak DA was obtained close to grasp onset, but all signal components, except for the intermediate-frequency range, provided significant information on grasp type almost over the entire duration of the trial, indicating that grasp type could be decoded already during the reaching movement.

Additionally, we evaluated whether grasp type could be significantly predicted before the start of the reaching movement, i.e., on average, 1.1 s before grasping (see Table 2), that is, in the absence of hand-arm movements while the subjects held their hand still in the initial resting position. To this end, we tested discrimination of the two grasp types based on 4 samples of each hand-arm motor channel, from time periods from 500 to 125 ms before movement onset, thereby excluding any possible sensory feedback from movement execution. For each subject, any of the four selected signal components (low-, intermediate- and high-frequency amplitudes and LFC) and all possible combinations thereof (15 combinations in total) were evaluated. Results from each subject were tested for significance ($p < 0.05$), Bonferroni-corrected for multiple testing (15 signal components and combinations). While DA was below this significance level for S1 and S2, three signal combinations yielded low but significant DA for S3 (above 58%, see supplementary material, Fig. SUP9 for details).

Anatomical origin of informative signals

Thus far, signals from the hand-arm motor cortex were used as features to classify ECoG recordings according to grasp type. Additionally, we determined the DA over all anatomical locations covered by the electrode arrays. For this purpose, we used a temporal pattern of features (as discussed in the previous section) from only a single electrode at a time and evaluated the DA of grasp types as it is shown for all three subjects in Fig. 6. We found that, for S1 and S3, the most informative sites were located in areas identified as part of the hand motor cortex by electrical stimulation. This held for all four analyzed signal components, although the specific contributions varied with the signal component used.

For S2, a slightly different picture emerged: only four electrodes in total were found to reside over the hand-arm motor cortex, and the most informative signals were found to originate from the somato-

sensory cortex. S2 also was the only subject in whom recordings were obtained from the left hemisphere and the only one to use the dominant hand. Whether these differences are a reason for the lower amount of grasp-specific information found in the recorded motor-cortical channels, however, would require further investigation in a larger sample of subjects to systematically compare dominant and non-dominant, as well as left and right hemisphere signals.

For S1 and S3, channels on somato-sensory areas showed the second highest capacity to discriminate between grasp types. For these two subjects, significant DAs up to 79% (high-frequency band, S3) could also be obtained from channels from Brodmann areas 44 and 45 (homologue of Broca's area in the right hemisphere). Significant DAs were also found for parts of the posterior parietal cortex (cf. Figs. 2 and 6) in all subjects. Brodmann areas 44 and 45 are known to be activated during both performed and imagined hand movements (Gerardin et al., 2000). The posterior parietal cortex has been shown to participate in appointing hand-shape and gripping force during visuo-motor tasks (Davare et al., 2007).

Influence of applied hand forces

In addition to decoding grasp type, we also classified cup weights as a separate property of each trial providing additional useful information. To assess the suitability of different frequency bands, we ran the same decoding procedure as for the classification of grasp types (cf. Fig. 3c), i.e., in a scan over all possible contiguous frequency bands, but now using features later in the trial (0.5 s before to 1 s after grasp time) to better represent the epoch of carrying the cup. Results are shown in Fig. SUP1 (supplementary material). According to this analysis, and compared to the earlier results in Fig. 3c, we found slightly different frequency bands than in the case of decoding grasp type to yield a high DA for cup weight: 0–10 Hz as a low-, 14–26 Hz as an intermediate-, and 74–118 Hz as a high-frequency band. These three frequency bands, and their possible combinations, together with the earlier described LFC, were subsequently compared for their performance in decoding cup weight. The results are summarized in Fig. 5c. The LFC was clearly the most informative signal component for all subjects, followed by amplitudes in the high-frequency band. Features yielding the highest DA could be found shortly before grasp onset and very late in the carrying phase (Fig. SUP2, supplementary material). Note that, in all cases, weight decoding yielded a

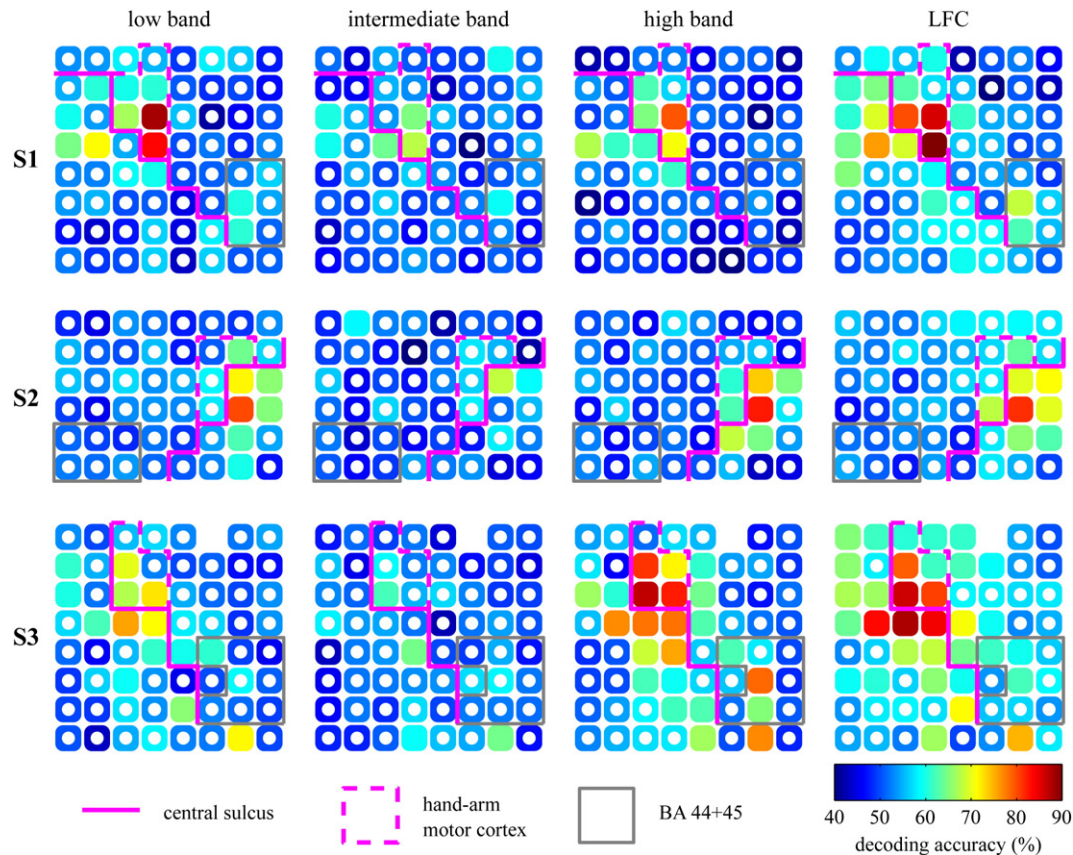


Fig. 6. Anatomical origin of informative signals. Results are exemplarily provided for S1, S2 and S3. The DA was computed using a temporal pattern of samples from each single electrode of the ECoG electrode grid. Results are color-coded for each electrode and arranged according to the electrode locations on the grid. Color patches with a central white dot indicate the DA below significance level ($p < 0.05$, Bonferroni-corrected for multiple testing). Solid magenta lines separate electrode positions posterior and anterior to the central sulcus; the dashed line outlines electrodes over the hand-arm motor area; a gray outline marks electrodes over Brodmann areas 44 and 45. The spatial mapping is presented separately for each of the examined signal components (from left to right: low-, intermediate- and high-frequency band amplitudes, and LFC).

substantially lower DA than grasp type decoding, even though the composition of feature vectors was adapted to each condition independently and in the same way.

One possible concern could be that, by using different grasp types and holding the cup at different positions, different forces might have been applied by the subject. Possibly, therefore, results presented in section "Classification of grasp types" might indicate the decoding of hand force rather than hand configuration during the grasp. Our experimental design, with half of the trials performed with a lightweight cup and the other half with a five times heavier version (cf. Methods), however, controls for this possibility: should we have mainly decoded hand force, variations in applied force across trials should, to a larger extent, be related to object weight than to grasp type. Results presented thus far did not distinguish between trials with a light or a heavy cup, indicating that grasp type can be inferred from ECoG independently of the grasped object's weight and, hence, of the associated variations in applied force.

To further investigate generalization of grasp decoding over different object weights, we trained the classifier for differentiating grasp type only on the basis of the trials with the heavy cup, using the most successful combination of ECoG signal components (low- and high-frequency band and LFC), and tested its decoding performance on the trials with the light cup, and vice versa. Average results, summarized in Table 3, were very similar to the ones obtained using an analogous two-fold cross-validation using 'weight-balanced trials', with equal amounts of trials with low and high weights in test and training data sets, respectively (Table 3). Although the decoding based on low-weight trials with a decoder trained on high-weight trials resulted in a somewhat lower DA than in the procedure performed the

other way round, this difference was small and only significant ($p < 0.05$) for S1 (Wilcoxon rank sum test, see Table 3 for p-values). Even in the case of S1, the average DA obtained in this manner (89.4%) was not much lower than the DA obtained when decoding with mixed-weight, weight-balanced trials in test and training set (95.3%).

In summary, our results indicate that the weight of the object – and, hence, the applied hand force – had, if at all, only a weak effect on the decoding of grasp type from the ECoG data.

Table 3

Control for effects of force (weight of the grasped object) on the generalization of grasp decoding. Row 1 ('trained on high weight') shows the decoding accuracy (DA, in %) when the classifier was only trained on trials executed with the heavier cup and then evaluated over the remaining trials i.e., while using the light-weight cup. Row 2 ('trained on low weight') shows DA for the opposite case. P-values are given to assess statistical significance for the difference between these two results by splitting up test sets into 15 subsets and comparing the distribution of both results with the Wilcoxon rank sum test. Feature vectors for decoding were constructed from a temporal pattern of all hand-arm motor channels, combining low- and high-frequency amplitudes, and the LFC (cf. Fig. 5a). For comparison of the average results for the transfer of decoding models across different weights ('average'), the bottom row ('weight-balanced trials') provides decoding results from a comparable two-fold cross-validation with equal numbers of low- and high-weight trials in test and training sets repeated and averaged over 20 different random realizations of validation subsets.

	S1	S2	S3
Trained on high weight	84.9	78.1	92.8
Trained on low weight	93.7	81.3	95.2
p-value	0.012	0.603	0.270
Average	89.4	79.7	94.0
Weight-balanced trials	95.3	81.0	95.1

Dependence on arm kinematics

From previous studies, it is known that arm kinematics as a continuous property of arm movements are represented in the ECoG and can be decoded with linear methods (Pistohl et al., 2008; Schalk et al., 2007), albeit with limited precision. If, alongside with finger kinematics, which define hand posture, also the kinematics of arm trajectories vary over different grasp types, part of the DA from ECoG signals could be explained by its relation to arm kinematics, rather than to hand postures.

Synchronously acquired recordings of wrist position did, indeed, reveal significant differences in arm kinematics for both grasp types, as represented by absolute position in the workspace (on the x-, y- and z-axis), velocity (in x-, y- and z-direction) and absolute hand speed (magnitude of the 3-dimensional velocity vector). Illustrations of these differences are provided as supplementary material (Fig. SUP7). To test how much influence these differences might have on the classification of grasp types – provided arm kinematics were perfectly represented in the ECoG – we tried decoding directly from a set of kinematic parameters of the arm movement, as a function of time, relative to the grasp. Generally, a feature vector including all examined kinematic parameters (3-dimensional position and velocity and absolute speed) delivered highest DA. The peak DA for pure arm-kinematics-based decoding was lower than that for the LFC alone, while not negligible in amplitude, and its time course was different (supplementary material, Fig. SUP8).

However, we were able to show that the DA achieved using ECoG did not require differences in the arm kinematics described above. To this end, for each subject, we selected the time of the maximum DA resulting from the 7-dimensional vector of movement parameters and subsequently searched for a subset of trials that minimized grasp-specific differences in arm kinematics at this particular time in the trial. This was done by eliminating trials to obtain equal (binned) distributions of kinematic parameters for both grasp types. In effect, the DA resulting from arm kinematics of this subset was not significant at $p < 0.01$. Subsequent decoding from the LFC on the same subset of trials (and at the same time) was unaffected in comparison to decoding on the complete trial set (see supplementary material, Fig. SUP8, for more detailed results), demonstrating that grasp types can be decoded from ECoG independently from arm velocity or position in the workspace.

Discussion

Movements examined in this study are of relevance for answering the question whether ECoG can provide control signals for a grasping prosthesis for paralyzed patients. Our motor task involved natural movement patterns. Movements relied on internal choices, i.e., in each trial, the timing of the movement sequence was self-paced and the choice of grasp type was made by the subject. Therefore, we decoded signals generated by the subjects' own intentions and actions, rather than by external commands.

Several sources of variability were included into the experiment, ensuring that the decoding could generalize over different task conditions and did not require a stereotyped grasping movement. While the degree of variability over different object weights and positions within the workspace was well controlled, other sources of variability were more implicit and due to the natural character of the grasping task, which, e.g., allowed for varying the exact position of the cup handle at the beginning of each trial. We found that, in spite of these variable conditions, grasp type could be inferred with high accuracy.

Comparison to other studies decoding grasp types and finger movements

Apart from evaluating the usefulness of ECoG signals for grasp decoding, this study aimed to establish a new approach to the

decoding of grasping movements by investigating (i) self-paced and, (ii) with respect to the type of grasp, self-chosen grasping movements that were (iii) part of a complex natural movement sequence (reaching for a cup, grasping and picking it up, then putting the cup down in a different position of the workspace). Such an approach appears particularly useful for BMI development, as BMI control should be self-initiated and work in natural conditions. In the following section, we establish a context of previous studies on related topics, applying different approaches.

It has been reported (Kubánek et al., 2009; Miller et al., 2009) that single finger movements are strongly correlated with a broadband component of the ECoG, including all frequencies up to 200 Hz. In these studies, neighboring electrodes showed preferences for different individual fingers.

On a smaller spatial scale, LFP recordings have been used to investigate grasp configurations. Mollazadeh et al. (2008) conducted a study in which instructed externally paced dexterous finger movements were performed by a monkey during the operation of three different switches, while LFP was measured from the motor cortex. Similar to our results, the type of hand movement could be decoded with highest accuracy from the spectral power in a high- (75–170 Hz) and low-frequency bands (<4 Hz), whereas signal components in intermediate-frequency ranges (6–15 Hz and 17–40 Hz) only yielded poor decoding. In this LFP study, average DAs up to 81% were reported based on the low- and high-frequency components from 10 electrodes by using a multi-layered artificial neural network.

Furthermore, Spinks et al. (2008), focusing on LFP power in 15–30 Hz and 30–50 Hz bands from the macaque primary motor cortex and area F5 during grasping of different objects, found differences during the grasping of an object grasped in different ways (e.g., hook and side grip). The choice of the analyzed frequency bands, in comparison to our study, is remarkable, as we found only very weak decoding within these frequency ranges. However, since no single-trial based decoding analysis was carried out, these results are not quantitatively comparable to those of our study.

Stark and Abeles (2007) analyzed the LFP, together with single-unit activity (SUA) and a multi-unit activity signal component that reflected an estimate of the activity of multiple neurons surrounding the electrode tip, calculated as the root mean square of 300–6000 Hz filtered extracellular potentials. These signals were recorded from the dorsal premotor cortex, while the monkeys grasped different objects from one of six positions after an instructed delay. Using LFP or SUA from up to 16 electrodes, two grasp types (power and precision grip) could be distinguished with a 73% accuracy in both cases. Using the multi-unit activity estimate, grasp type could be decoded with an 85% accuracy.

A comparison of our results to these studies, as far as such a comparison is possible in view of differences in experimental design, indicates that ECoG recordings from the human motor cortex are, in terms of the DA of different grasp types, on par with LFP and spike recordings from intra-cortical microelectrodes. This is in contrast with previous observations that the decoding of reaching direction or arm movement trajectories is considerably less accurate from ECoG, compared to SUA, MUA or LFP (e.g., Pistohl et al., 2008; Schalk et al., 2007 for ECoG, and Wu et al., 2006 for SUA; see also Waldert et al., 2009 for a comparison).

One possible explanation for this difference between grasp decoding and arm movement decoding may be found in the spatial scale of neuronal signals that are informative about different grasps and arm movements into different directions (cf., Fig. 6). Hand/finger representations in the human precentral motor cortex are particularly large and span several cm of the cortex along the central sulcus. Furthermore, the control of grasping movements involves interaction of a bigger number of joints and muscles. It is conceivable, therefore, that specific grasp configurations employ synergies between different, possibly distant, neuronal populations within the hand-arm area of

the motor cortex, which are all needed for accurate classification. Thus, the fact that ECoG electrode grids, as used in the present study, covering a relatively large area of the cortex might be advantageous in this case. Intra-cortical microelectrodes record mostly from a local neural population in a range up to millimeters, which is smaller than the area of the cortex covered by typical ECoG macro-electrodes. Therefore, if the differential neural activity patterns related to different arm movement directions predominate on a finer spatial scale than those related to different grasp types, they might be better captured in micro-electrode data.

Another explanation for the rather good performance of grasp type decoding from human ECoG compared to intra-cortical recordings in monkeys might be found in differences in the representation of hand and arm movements between humans and monkeys (Meier et al., 2008), in spite of the fact that comparisons of somatotopic maps of both species reveal many similarities. Also, dexterous grasping for humans constitutes a natural task which can be performed without any practice, while a similar task for monkeys usually relies on very specific, over-trained movements, a fact that could contribute to differences in cortical representation.

Decoded signal components

During the examination of ECoG related to grasping movements, most of the discriminative power could be found in slow modulations (represented by the LFC), as they can also be observed in averages of neural signals in the time domain, as well as in amplitude modulations in high frequencies above about 55 Hz. The range of low-frequency amplitude modulations that yielded a high DA overlapped with the frequency content of the time-domain LFC, and may, to a large extent, reflect activation of the same neuronal ensembles. The suppression of sensorimotor rhythms in an intermediate-frequency range was spatially widespread and consistently observed over both subjects and trials. Its specificity for grasp types was, however, weak (see Figs. 3 and 5). These observations are in good agreement with previous reports about the decoding of movement direction from MEG (Waldert et al., 2008), ECoG (Ball et al., 2009a; Schalk et al., 2007) and from the LFP (Rickert et al., 2005).

The functional significance of this high-frequency ECoG component is currently under intense debate (Crone et al., 2011). There is accumulating evidence that the high-frequency ECoG is a suitable index for functional mapping (Jerbi et al., 2000; Schalk et al., 2008b) and is indicative of memory- and attention-related functions (Brovelli et al., 2005; Jensen et al., 2007). It has been suggested that low- and high-frequency responses observed in the ECoG of the motor cortex are, in fact, part of a broad-band signal component, the contiguity of which is masked by the prominent rhythms in intermediate alpha- and beta-frequency ranges (Miller et al., 2009). In our study, task-related activity in low and high frequencies (cf. Fig. 3a), as well as the informative content of the LFC and low- and high-frequency amplitudes do, to a great extent, overlap – both temporally (Fig. 5b) and spatially (Fig. 6). However, together with the previous observation of different preferred directions for the LFC and gamma-band activity (Ball et al., 2009a), the observation that a combination of these signal components did consistently increase the DA in all subjects suggests that – to some degree – both signal components may reflect functionally different neural processes.

Sensory and attentional factors

We only used signals from electrodes in direct contact with regions of the motor cortex that, during electrical stimulation, evoked motor hand and arm responses. Thus, it is unlikely that post-central sensory processing was the exclusive source of the decoded signals. However, as proprioceptive information is projected to the motor cortex (Naito et al., 1999), and considering the fact that, due to volume conduction,

neural sources can be still detected in neighboring locations by ECoG, as demonstrated by analyses of source visibility (Dümpelmann et al., 2011), it is not to be excluded that the afferent information could be responsible for part of the decoded signals.

Our task design did not involve an explicit planning phase for which movement intentions could be studied in the absence of movement. Since our results were aimed to be relevant for future implementation in free BMI control, we designed a task in which classification of signals did not rely on external cues or artificially separated movement components (e.g., isolated reach and isolated grasp). Absence of overt hand and arm motion and, hence, possible proprioceptive feedback was thus only given within an inter-trial resting period, long before the actual grasp (1.1 ± 0.3 s). An additional decoding analysis based on signals from this time period yielded a very weak DA, exceeding the significance level ($p < 0.05$) for only one subject (supplementary material, Fig. SUP9).

Apart from proprioceptive interference, other sensory modalities could have played a role, too. About 20% of neurons in the primary motor cortex show significant responses to visual stimuli, and some of these neurons modulate their firing behavior with respect to position or motion of visual stimuli, which may be important for visuo-motor coordination (Merchant et al., 2001). Furthermore, different demands of visuo-motor processing for both grasp types (a precision grip requires finer visuo-motor coordination than a whole-hand grip) could have had an effect on the measured signals from the motor cortex. This, however, does not necessarily constitute a confounding factor in the analysis, but may rather form an integral part of movement preparation and visuo-motor planning investigated in the present study and therefore this kind of neuronal signals might also be available during brain-machine interface control of a grasping prosthesis. Signals related to visuo-motor planning from the posterior parietal cortex have been already considered as viable candidates for brain-machine interfacing (Scherberger et al., 2005).

On the other hand, differential activity in response to pure movement observation – and, hence, unrelated to motor processing – can be found in areas that are associated with movement execution. These are mainly found in the ventral premotor cortex and the anterior intraparietal cortex (Dinstein et al., 2008), the latter of which has specifically been reported to code for complexity of the hand movements observed (Biagi et al., 2010). None of the signals included into our main analyses were recorded from these areas. Observation of one's own movement could, however, explain the decoding possible from posterior parietal locations and Brodmann areas 44/45 (see Fig. 6).

Grasp type may coincide with other differential movement properties not controlled for in our experimental paradigm. For instance, we have observed that, in whole-hand grip trials, the speed of arm movements was higher and movement duration was slightly shorter than during precision grips (Fig. SUP 7, supplementary material). While we could exclude that differential arm kinematics are a prerequisite for an accurate classification of grasp types (Section 3.5), different levels of task difficulty, and hence potentially different attentional demands could have played a role in the applied task: precision and whole-hand grips require different levels of fine-tuning in the pre-shaping of the hand, which may require different levels of visuo-spatial and motor attention. Neural systems involved in attentional processing comprise widespread fronto-parietal networks (Driver et al., 2010; Rushworth et al., 2003). Functional imaging studies suggest that motor attention also modulates cortical activity in the primary motor cortex (Binkofski et al., 2002; Johansen-Berg and Matthews, 2002), and processing of visuo-spatial attention has been associated with high-frequency activity in the ECoG recorded on the premotor cortex (Brovelli et al., 2005). Thus, it cannot be excluded that differences in attentional demands might have contributed to the differential ECoG signals we used for grasp-type decoding. To clarify the role of attentional processing in different types of movements,

including grasping, further behavioral and brain research, beyond the scope of the present investigation, is necessary. However, if differential attention-related signals are difficult to disentangle from movement-related activity, the corresponding attentional demands might be closely linked to the performance of different grasp types, thus being informative for grasp type decoding. Therefore, the different degrees of attention required for different types of motor performances might ultimately not confound, but support the use in BMI applications.

Relevance for BMIs

We have shown that it is possible to decode natural grasp types from motor-cortical ECoG signals with high accuracy. As grasping forms a necessary part of everyday human motor behavior, these results are a significant step towards an ECoG-based BMI which would allow for the neuronal control of grasping movements by paralyzed people. The high accuracy of our decoding may encourage testing classification of a higher number of grasp types (e.g., hook grips, grasping along horizontal vs. vertical axes).

It would certainly be preferable if grasp types could be decoded by non-invasive means like EEG or MEG. The feasibility of asynchronous EEG-based BMIs controlled by voluntary modulations of EEG activity has been impressively demonstrated (McFarland et al., 2010). Control strategies for these BMIs often involve neural activity related to movement execution or imagination of movements of different body parts with spatially separate representations in the motor cortex (e.g., Blankertz et al., 2007; Neuper et al., 2006). Only recently, some studies tried to decode different movements of the same limb from non-invasive recordings (Bradberry et al., 2009, 2010; Waldert et al., 2008). Decoding of movement direction from MEG and EEG has been reported to reach only about half the information transfer rate as for directional movement decoding from ECoG signals (cf. Ball et al., 2009a; Waldert et al., 2008, 2009). In the present study, some EEG channels were recorded at the same time as ECoG, allowing for a first direct comparison of invasive and non-invasive signals. Using the few EEG channels available, classification of different grasp types was possible, to some degree, in two out of three subjects, but the DA obtained (55.5–63%) was much lower than in the ECoG data (see supplementary material, Fig. SUP10). An explanation of such low performance might be the inferior spatial resolution and lower signal-to-noise ratio of the EEG. We suspect that EEG recordings in the present form, with current analysis approaches, might, in fact, have a limited capacity for discriminating different grasping movements.

There are several further requirements that would have to be fulfilled by a BMI in order to provide adequate commands for grasping that have not been addressed in this study. One step of fundamental importance will be to show that the time of grasp onset can be inferred from neuronal data with sufficient accuracy. Other concerns are whether and how a classifier could be trained without actual movements in order to be applicable in patients for whom a BMI would primarily be designed, i.e., patients with missing limbs or suffering from paralysis. Moreover, for some practical applications, considering modulations of the gripping force might also be necessary. Furthermore, as successful grasping requires correct release of the grasp, it still needs to be clarified whether a command for sustained grasping or a separate command for object release (extension of fingers, rather than flexion) would be better suited for a natural and intuitive BMI-based control of a grasping movement.

In spite of the fact that these various issues still require further investigation, the presented results indicate that neural population activity recorded from the cortical surface could be a potential candidate for use in the restoration (or replacement) of grasping movements via BMI technology.

Acknowledgments

This work was funded by the German Federal Ministry of Education and Research (BMBF grants 01GQ0420 to BCCN Freiburg and GoBio 0313891).

Appendix A. Supplementary data

Supplementary data to this article can be found online at doi:10.1016/j.neuroimage.2011.06.084.

References

- Ball, T., Nawrot, M.P., Pistohl, T., Aertsen, A., Schulze-Bonhage, A., Mehring, C., 2004. Towards an implantable brain-machine interface based on epicortical field potentials. *Biomed. Technik* 49, 756–759.
- Ball, T., Schulze-Bonhage, A., Aertsen, A., Mehring, C., 2009a. Differential representation of arm movement direction in relation to cortical anatomy and function. *J. Neural Eng.* 6, 016006.
- Ball, T., Kern, M., Mutschler, I., Aertsen, A., Schulze-Bonhage, A., 2009b. Signal quality of simultaneously recorded invasive and non-invasive EEG. *NeuroImage* 46, 708–716.
- Biagi, L., Cioni, G., Fogassi, L., Guzzetta, A., Tosetti, M., 2010. Anterior intraparietal cortex codes complexity of observed hand movements. *Brain Res. Bull.* 81, 434–440.
- Binkofski, F., Fink, G.R., Geyer, S., Buccino, G., Gruber, O., Shah, N.J., Taylor, J.G., Seitz, R.J., Zilles, K., Freund, H.J., 2002. Neural activity in human primary motor cortex areas 4a and 4p is modulated differentially by attention to action. *J. Neurophysiol.* 88, 514–519.
- Blankertz, B., Dornhege, G., Krauledat, M., Müller, K.R., Curio, G., 2007. The non-invasive Berlin Brain-Computer Interface: fast acquisition of effective performance in untrained subjects. *NeuroImage* 37, 539–550.
- Bradberry, T.J., Rong, F., Contreras-Vidal, J.L., 2009. Decoding center-out hand velocity from MEG signals during visuomotor adaptation. *NeuroImage* 47, 1691–1700.
- Bradberry, T.J., Gentili, R.J., Contreras-Vidal, J.L., 2010. Reconstructing three-dimensional hand movements from noninvasive electroencephalographic signals. *J. Neurosci.* 30, 3432–3437.
- Brovelli, A., Lachaux, J.P., Kahane, P., Boussaoud, D., 2005. High gamma frequency oscillatory activity dissociates attention from intention in the human premotor cortex. *NeuroImage* 28, 154–164.
- Carmena, J.M., Lebedev, M.A., Crist, R.E., O'Doherty, J.E., Santucci, D.M., Dimitrov, D.F., Patil, P.G., Henriquez, C.S., Nicolelis, M.A.L., 2003. Learning to control a brain-machine interface for reaching and grasping by primates. *PLoS Biol.* 1, 193–208.
- Chao, Z.C., Nagasaka, Y., Fujii, N., 2010. Long-term asynchronous decoding of arm motion using electrocorticographic signals in monkeys. *Front. Neuroeng.* 3, 3.
- Crone, N.E., Korzeniewska, A., Franszczuk, P.J., 2011. Cortical gamma responses: searching high and low. *Int. J. Psychophysiol.* 79, 9–15.
- Davare, M., Andres, M., Clerget, E., Thonnard, J.L., Olivier, E., 2007. Temporal dissociation between hand shaping and grip force scaling in the anterior intraparietal area. *J. Neurosci.* 27, 3974–3980.
- Dinstein, I., Gardner, J.L., Jazayeri, M., Heeger, D.J., 2008. Executed and observed movements have different distributed representations in human aIPS. *J. Neurosci.* 28, 11231–11239.
- Driver, J., Blankenburg, F., Bestmann, S., Ruff, C.C., 2010. New approaches to the study of human brain networks underlying spatial attention and related processes. *Exp. Brain Res.* 206, 153–162.
- Dümpelmann, M., Ball, T., Schulze-Bonhage, A., 2011. sLORETA allows reliable distributed source reconstruction based on subdural strip and grid recordings. *Hum. Brain Mapp.* doi:10.1002/hbm.21276
- Eickhoff, S.B., Heim, S., Zilles, K., Amunts, K., 2006. Testing anatomically specified hypotheses in functional imaging using cytoarchitectonic maps. *NeuroImage* 32, 570–582.
- Friedman, J.H., 1989. Regularized discriminant analysis. *J. Am. Stat. Assoc.* 84, 165–175.
- Gerardin, E., Sirigu, A., Lehericy, S., Poline, J.B., Gaymard, B., Marsault, C., Agid, Y., Le Bihan, D., 2000. Partially overlapping neural networks for real and imagined hand movements. *Cereb. Cortex* 10, 1093–1104.
- Gunduz, A., Sanchez, J.C., Carney, P.R., Principe, J.C., 2009. Mapping broadband electrocorticographic recordings to two-dimensional hand trajectories in humans: Motor control features. *Neural Netw.* 22, 1257–1270.
- Hastie, T., Buja, A., Tibshirani, R., 1995. Penalized discriminant analysis. *Ann. Stat.* 23, 73–102.
- Jensen, O., Kaiser, J., Lachaux, J.P., 2007. Human gamma-frequency oscillations associated with attention and memory. *Trends Neurosci.* 30, 317–324.
- Jerbi, K., Ossandón, T., Hamamé, C.M., Senova, S., Dalal, S.S., Jung, J., Minotti, L., Bertrand, O., Berthoz, A., Kahane, P., Lachaux, J.P., 2009. Task-related gamma-band dynamics from an intracerebral perspective: review and implications for surface EEG and MEG. *Hum. Brain Mapp.* 30, 1758–1771.
- Jerbi, K., Lachaux, J.P., N'Diaye, K., Pantazis, D., Leahy, R.M., Garnero, L., Baillet, S., 2007. Coherent neural representation of hand speed in humans revealed by MEG imaging. *Proc. Natl. Acad. Sci. U. S. A.* 104, 7676–7681.
- Johansen-Berg, H., Matthews, P.M., 2002. Attention to movement modulates activity in sensori-motor areas, including primary motor cortex. *Exp. Brain Res.* 142, 13–24.
- Kovalev, D., Spreer, J., Honegger, J., Zentner, J., Schulze-Bonhage, A., Huppertz, H.J., 2005. Rapid and fully automated visualization of subdural electrodes in the presurgical evaluation of epilepsy patients. *AJNR Am. J. Neuroradiol.* 26, 1078–1083.

- Kubánek, J., Miller, K.J., Ojemann, J.G., Wolpaw, J.R., Schalk, G., 2009. Decoding flexion of individual fingers using electrocorticographic signals in humans. *J. Neural Eng.* 6, 066001.
- Lal, T.N., Schröder, M., Hinterberger, T., Weston, J., Bogdan, M., Birbaumer, N., Schölkopf, B., 2004. Support vector channel selection in BCI. *IEEE Trans. Biomed. Eng.* 51, 1003–1010.
- Leuthardt, E.C., Schalk, G., Wolpaw, J.R., Ojemann, J.G., Moran, D.W., 2004. A brain-computer interface using electrocorticographic signals in humans. *J. Neural Eng.* 1, 63–71.
- Leuthardt, E.C., Miller, K.J., Schalk, G., Rao, R.P., Ojemann, J.G., 2006. Electrocorticography-based brain computer interface – the Seattle experience. *IEEE Trans. Neural Syst. Rehabil. Eng.* 14, 194–198.
- Levine, S.P., Huggins, J.E., BeMent, S.L., Kushwaha, R.K., Schuh, L.A., Rohde, M.M., Passaro, E.A., Ross, D.A., Elisevich, K.V., Smith, B.J., 2000. A direct brain interface based on event-related potentials. *IEEE Trans. Rehabil. Eng.* 8, 180–185.
- Mason, C.R., Gomez, J.E., Ebner, T.J., 2001. Hand synergies during reach-to-grasp. *J. Neurophysiol.* 86, 2896–2910.
- McFarland, D.J., Sarnacki, W.A., Wolpaw, J.R., 2010. Electroencephalographic (EEG) control of three-dimensional movement. *J. Neural Eng.* 7, 036007.
- Mehring, C., Rickert, J., Vaadia, E., Cardoso de Oliveira, S., Aertsen, A., Rotter, S., 2003. Inference of hand movements from local field potentials in monkey motor cortex. *Nat. Neurosci.* 6, 1253–1254.
- Mehring, C., Nawrot, M.P., Cardoso de Oliveira, S., Vaadia, E., Schulze-Bonhage, A., Aertsen, A., Ball, T., 2004. Comparing information about arm movement direction in single channels of local and epicortical field potentials from monkey and human motor cortex. *J. Physiol. (Paris)* 98, 498–506.
- Meier, J.D., Aflalo, T.N., Kastner, S., Graziano, M.S., 2008. Complex organization of human primary motor cortex: a high-resolution fMRI study. *J. Neurophysiol.* 100, 1800–1812.
- Merchant, H., Battaglia-Mayer, A., Georgopoulos, A.P., 2001. Effects of optic flow in motor cortex and area 7a. *J. Neurophysiol.* 86, 1937–1954.
- Miller, K.J., Zanos, S., Fetz, E.E., den Nijs, M., Ojemann, J.G., 2009. Decoupling the cortical power spectrum reveals real-time representation of individual finger movements in humans. *J. Neurosci.* 29, 3132–3137.
- Mollazadeh, M., Aggarwal, V., Singhal, G., Law, A., Davidson, A., Schieber, M., Thakor, N., 2008. Spectral modulation of LFP activity in M1 during dexterous finger movements. 30th Annual International IEEE EMBS Conference, pp. 5314–5317.
- Moritz, C.T., Perlmutter, S.I., Fetz, E.E., 2008. Direct control of paralysed muscles by cortical neurons. *Nature* 456, 639–643.
- Müller, T., Ball, T., Kristeva-Feige, R., Mergner, T., Timmer, J., 2000. Selecting relevant electrode positions for classification tasks based on the electro-encephalogram. *Med. Biol. Eng. Comput.* 38, 62–67.
- Naito, E., Ehrsson, H.H., Geyer, S., Zilles, K., Roland, P.E., 1999. Illusory arm movements activate cortical motor areas: a positron emission tomography study. *J. Neurosci.* 19, 6134–6144.
- Neuper, C., Müller-Putz, G.R., Scherer, R., Pfurtscheller, G., 2006. Motor imagery and EEG-based control of spelling devices and neuroprostheses. *Prog. Brain Res.* 159, 393–409.
- Percival, D.B., Walden, A.T., 1993. *Spectral Analysis for Physical Applications*. Chapter 7, Cambridge University Press.
- Pistohl, T., Ball, T., Schulze-Bonhage, A., Aertsen, A., Mehring, C., 2008. Prediction of arm movement trajectories from ECoG-recordings in humans. *J. Neurosci. Meth.* 167, 104–114.
- Ramoser, H., Müller-Gerking, J., Pfurtscheller, G., 2000. Optimal spatial filtering of single trial EEG during imagined hand movement. *IEEE Trans. Rehabil. Eng.* 8, 441–446.
- Rickert, J., Cardoso de Oliveira, S., Vaadia, E., Aertsen, A., Rotter, S., Mehring, C., 2005. Encoding of movement direction in different frequency ranges of motor cortical local field potentials. *J. Neurosci.* 25, 8815–8824.
- Rumeau, C., Tzourio, N., Murayama, N., Peretti-Viton, P., Levrier, O., Joliot, M., Mazoyer, B., Salamon, G., 1994. Location of hand function in the sensorimotor cortex: MR and functional correlation. *AJNR Am. J. Neuroradiol.* 15, 567–572.
- Rushworth, M.F., Johansen-Berg, H., Göbel, S.M., Devlin, J.T., 2003. The left parietal and premotor cortices: motor attention and selection. *NeuroImage* 20, S89–S100.
- Santello, M., Soechting, J.F., 2000. Force synergies for multifingered grasping. *Exp. Brain Res.* 133, 457–467.
- Savitzky, A., Golay, J.E., 1964. Smoothing and differentiation of data by simplified least squares procedures. *Anal. Chem.* 36, 1627–1639.
- Schalk, G., Kubánek, J., Miller, K.J., Anderson, N.R., Leuthardt, E.C., Ojemann, J.G., Limbrick, D., Moran, D., Gerhardt, L.A., Wolpaw, J.R., 2007. Decoding two-dimensional movement trajectories using electrocorticographic signals in humans. *J. Neural Eng.* 4, 264–275.
- Schalk, G., Miller, K.J., Anderson, N.R., Wilson, J.A., Smyth, M.D., Ojemann, J.G., Moran, D.W., Wolpaw, J.R., Leuthardt, E.C., 2008a. Two-dimensional movement control using electrocorticographic signals in humans. *J. Neural Eng.* 5, 75–84.
- Schalk, G., Leuthardt, E.C., Brunner, P., Ojemann, J.G., Gerhardt, L.A., Wolpaw, J.R., 2008b. Real-time detection of event-related brain activity. *NeuroImage* 43, 245–249.
- Scherberger, H., Jarvis, M.R., Andersen, R.A., 2005. Cortical local field potential encodes movement intentions in the posterior parietal cortex. *Neuron* 46, 347–354.
- Schieber, M.H., Hibbard, L.S., 1993. How somatotopic is the motor cortex hand area? *Science* 261, 489–492.
- Spinks, R.L., Kraskov, A., Brochier, T., Umiltà, M.A., Lemon, R.N., 2008. Selectivity for grasp in local field potential and single neuron activity recorded simultaneously from M1 and F5 in the awake macaque monkey. *J. Neurosci.* 28, 10961–10971.
- Stark, E., Abeles, M., 2007. Predicting movement from multiunit activity. *J. Neurosci.* 27, 8387–8394.
- Steinmetz, H., Furst, G., Meyer, B.U., 1989. Craniocerebral topography within the international 10–20 system. *Electroencephalogr. Clin. Neurophysiol.* 72, 499–506.
- Taylor, D.M., Tillery, S.I., Schwartz, A.B., 2002. Direct cortical control of 3D neuroprosthetic devices. *Science* 296, 1829–1832.
- Thakur, P.H., Bastian, A.J., Hsiao, S.S., 2008. Multidigit movement synergies of the human hand in an unconstrained haptic exploration task. *J. Neurosci.* 28, 1271–1281.
- Thomson, D.J., 1982. Spectrum estimation and harmonic analysis. *Proc. IEEE* 70, 1055–1096.
- Velliste, M., Perel, S., Spalding, M.C., Whitford, A.S., Schwartz, A.B., 2008. Cortical control of a prosthetic arm for self-feeding. *Nature* 453, 1098–1101.
- Waldert, S., Preissl, H., Demandt, E., Braun, C., Birbaumer, N., Aertsen, A., Mehring, C., 2008. Hand movement direction decoded from MEG and EEG. *J. Neurosci.* 28, 1000–1008.
- Waldert, S., Pistohl, T., Braun, C., Ball, T., Aertsen, A., Mehring, C., 2009. A review on directional information in neural signals for brain-machine interfaces. *J. Physiol. (Paris)* 103, 244–254.
- Wu, W., Gao, Y., Bienenstock, E., Donoghue, J.P., Black, M.J., 2006. Bayesian population decoding of motor cortical activity using a Kalman filter. *Neural Comput.* 18, 80–118.
- Yousry, T.A., Schmid, U.D., Alkadhi, H., Schmidt, D., Peraud, A., Buettner, A., Winkler, P., 1997. Localization of the motor hand area to a knob on the precentral gyrus. A new landmark. *Brain* 120, 141–157.
- Zatsiorsky, V.M., Li, Z.M., Latash, M.L., 2000. Enslaving effects in multi-finger force production. *Exp. Brain Res.* 131, 187–195.